International Journal of Environmental Sciences
ISSN: 2229-7359
Vol. 11 No. 21s, 2025
https://www.theaspd.com/ijes.php

Effect of Cobalt co-doping on Ionic Conductivity of $Co_y Gd_{x-y} Ce_{1-x} O_{2-\delta}$ and $Co_y Nd_{x-y} Ce_{1-x} O_{2-\delta}$ (y = 0.05 and 0.1 mol%) Nanocomposites Synthesized by EDTA-Glycol method.

Dr. A. S Tale[1*], Dr.S.D. Thakare[2], Mr.S.B. Deshmukh[3], Dr.M.J. Pawar[4] ,Dr.S.V. Jagtap[5]
[1*]Department of Applied Sciences & Humanities, Shri Sant Gajanan Maharaj College of Engineering Shegaon, Maharashtra.
[2]Department of Applied Sciences & Humanities Dr. Rajendra Gode Institute of Technology & Research, Amravati, Maharashtra.
[3]Department of Chemistry, ACS College, Kiran Nagar, Amravati, Maharashtra
[4]Department of Chemistry, ACS College, Kiran Nagar, Amravati, Maharashtra
[5]Department of Physics, R. D. I. K. & K. D. College, Badnera (Rly), Amravati, Maharashtra

Abstract
Cobalt co-doped ceria-based samples with composition of $Co_yGd_{x-y}Ce_{1-x}O_{2-\delta}$ and $Co_yNd_{x-y}Ce_{1-x}O_{2-\delta}$ (y = 0.05 and 0.1 mol%), have been prepared by EDTA-Glycol method and characterized to explore their use as a solid electrolyte material. Crystal structure, microstructure, and ionic conductivity have been characterized by X-ray diffraction, scanning electron microscopy, and impedance spectroscopy respectively. All the compositions have been found to be single phase with average crystallite size between 18-32 nm. Density of all the compositions is more than 97.50% of the theoretical value for all the doped and co-doped compositions. Results show that the samples cobalt co-doped exhibit higher ionic conductivity than the samples singly doped with Gd and Nd ions. At 600°C, the sample $Co_{0.1}Gd_{0.1}Ce_{0.8}O_{2-\delta}$ and $Co_{0.05}Nd_{0.15}Ce_{0.8}O_{2-\delta}$ exhibits maximum total conductivity 0.0166 Scm^{-1} and 0.0134 Scm^{-1} respectively.
Keywords: *Cobalt co-doped ceria, Nanocomposites, EDTA-Glycol method, ionic conductivity, Electrolyte.*

1.INTRODUCTION

Solid oxide fuel cells (SOFCs) have high power generating efficiency and applicable to a wide range of power supplies, from small scale distribution power supplies to large scale thermal power generation. Low pollution, high power densities, flexibility in using hydrocarbon fuels are the advantages of SOFC [1]. SOFC operating at intermediate temperature (< 800°C) has received increasing attention as the low operating temperatures prolongs the service life of SOFC and reduce the cost of materials processing and cell fabrication [2]. Solid oxide electrolyte is a key component of SOFCs that affect the cell performance and the operating temperature to a large extent. Solid oxide electrolytes based on ceria doped materials with sufficient electrical properties are being studied as the promising candidate materials for use in intermediate temperature solid oxide fuel cells (IT-SOFCs).

At present, doped ceria with cubic structure possesses highest ionic conductivity in the range of 450-750°C. High ionic conductivity in doped ceria is arises from charge compensating oxygen vacancies related to aliovalent cation conditions [3]. Ceria based solid electrolytes doped with various cations like La^{3+}, Gd^{3+}, Sm^{3+}, Pr^{3+} etc., at various dopant concentrations has been extensively investigated in order to get the electrolyte of high ionic conductivity at reduced temperature. Trivalent cation enhances the chemical stability, the ionic conductivity and suppresses the reducibility of ceria-based materials. Among the various dopants studied, gadolinia doped ceria (GDC) and samarium doped ceria (SDC) have been reported to have the highest ionic conductivity [4]. SDC materials shows high ionic conductivity [5-7], this is because, as a dopant Sm^{3+} cations minimizes the change in ceria lattice. Other than singly doped ceria, many studies have been reported on co-doped samples and results suggest that co-doping may enhance conductivity even at moderate or intermediate temperatures [8-11]. Ceria-based electrolytes, especially when doped with aliovalent cations (Gd or Sm) or co-doped with other rare-earth elements (i.e., Pr, Er, Nd) or earth-alkaline elements (i.e., Co, Ca, Sr). These allow for an increase in the overall concentration of oxygen vacancies and a tuning of their final electrochemical properties [2,3,4,5]. Co-doping of ceria has been found to be very effective for enhancement of conductivity in recent years [27–37]. Most of the co-dopants in these compounds contain d- block elements as a constituent.

Oxides of transition metal (e.g. Fe_2O_3, Co_2O_3, SrO_2, etc.) are some of the co-dopants suggested for decreasing the sintering temperature as well as enhancing the ionic conductivity of ceria-based solid electrolytes. Co has

previously been suggested as a sintering aid for CeO_2 [12]. M.A. *Azimova* et al. reported that co-doping is an effective technique for reducing the required sintering temperature to form dense ceramics and enhance the conductivity of ceria-based electrolytes [13]. In this work, cobalt co-doped $Ce_{0.9}Sm_{0.1}O_{2-\delta}$ nanopowders were synthesized. *Mori* et al. [11] reported that the ionic conductivity of $(La_{0.75}Sr_{0.2}Ba_{0.05})_{0.175}Ce_{0.825}O_{1.891}$ was higher than that of the respective singly doped ceria, and even that of CSO. Similarly, *Van Herle* et al. [6] found that co-doped ceria with three, five, or ten dopants showed significantly higher conductivity in air (by 10–30%) than the best singly- doped materials with the same oxygen vacancy concentration.

In the present work, in order to develop ceria-based electrolyte material, Co^{2+} co-doped ceria-based nanocomposite materials of compositions CoyGdx-yCe1-xO2-δ and CoyNdx-yCe1-xO2-δ (y = 0.05 and 0.1 mol%) were prepared by using EDTA-Glycol method and the as- prepared materials were characterized by XRD, SEM and UV-vis spectroscopy. The effect of the Co2O3 co-doping on crystallite size, relative density and activation energy were investigated. Effects of co- doping on the structure and electrical conductivity were studied in the temperature range of 300–800 ^{O} C.

2.Experimental

2.1 Method of synthesis

The pure CeO2 and $Co_yGd_{x-y}Ce_{1-x}O_{2-\delta}$ and $Co_yNd_{x-y}Ce_{1-x}O_{2-\delta}$ materials were used by a modified EDTA-Glycol method [14]. The highly pure Ce (NO3)3.6H2O, Gd (NO3)3.6H2O, Nd (NO3)3. 6H2O and Co(NO3)2.6H2O were used as the precursors. These salts were mixed independently in de-ionized water. Later on, all the solutions were mixed in the correct ratio in order to form the solid solution of $Co_yGd_{x-y}Ce_{1-x}O_{2-\delta}$ and $Co_yNd_{x-y}Ce_{1-x}O_{2-\delta}$ (y = 0.05 and 0.1 mol%) composition. The calculated quantity of ethylenediaminetetraacetic acid (EDTA), dilute ammonia and ethylene glycol (EG) was added to the nitrate solution. As obtained solution was stirred and kept on a hot plate for heat treatment at 80°C which in turn forms a gel-like mass. The resulted mass was combusted at 300°C for 2 hr followed by the calcination at 650°C for 7 hr to get final product in powder form. The calcined ceria-based powders; pure CeO_2, $Gd_{0.2}Ce_{0.8}O_{2-\delta}$, $Gd_{0.1}Ce_{0.8}O_{2-\delta}$,$Co_{0.1}Gd_{0.1}Ce_{0.8}O_{2-\delta}$,$Nd_{0.2}Ce_{0.8}O_{2-\delta}$, $Co_{0.05}$ $Nd_{0.15}Ce_{0.8}O_{2-\delta}$ and $Co_{0.1}Nd_{0.1}Ce_{0.8}O_{2-\delta}$ were coded as CE, GC, CGC05, CGC1, NC, CNC05 and CNC1 respectively. On calcination, the obtained ashes were ground in agate mortar to get fine homogeneous powders. Powder materials were uniaxially pressed into pellets with 6 mm of diameter and 2 mm thickness, at 200 MPa. Sintering was performed in air for 10 h at a constant heating rate of 2°C/min in between 1150°C to 1250°C.

2.2 Characterization

Phase composition was examined by X-ray diffraction (XRD). The values of specific surface areas (S_{BET}) of the calcined powders were measured by Brunauer-Emmett-Teller (BET) nitrogen-gas adsorption method. The densities of green and sintered pellets were calculated from the mass and dimensions of the samples, and measured using Archimedes method in a water bath. The microstructures of the powders and sintered samples were examined in a scanning electron microscope (SEM). The average grain size was measured by the intercept method on the surface of polished and thermally etched sintered samples. The size of at least 300 grains was considered. For electrical measurements, impedance spectroscopy was performed on sintered pellets of four samples CE, GC, CGC05, CGC1, NC, CNC05 and CNC1. The pellets were made by pressing 4 g of powder at 200 MPa in a 25 mm die and were sintered for 6 hours at the temperatures 1150°C and 1250°C. The densities of pellets pressed and sintered at 1250°C for 6 h as described above were determined from their mass and dimensions. For electrical measurements, silver contacts were applied on both the flat surfaces and cured at 500°C for 15 min. An impedance analyzer (KEYSIGHT-E4990A) was used to characterize the impedance spectra of sintered samples in the static ambient atmosphere in the frequency range 20 Hz to 5 MHz from 550 to 950°C. The spectra were fitted using the Zsimpwin software and values for the total, bulk and grain boundary conductivities were noted.

3. RESULTS AND DISCUSSION

3.1 XRD

All the CeO_2, $Gd_{0.2}Ce_{0.8}O_{2-\delta}$, $Gd_{0.1}Ce_{0.8}O_{2-\delta}$, $Co_{0.1}Gd_{0.1}Ce_{0.8}O_{2-\delta}$, $Nd_{0.2}Ce_{0.8}O_{2-\delta}$, $Co_{0.05}$ $Nd_{0.15}Ce_{0.8}O_{2-\delta}$ and $Co_{0.1}Nd_{0.1}Ce_{0.8}O_{2-\delta}$ powders were characterized by X-ray diffraction techniques and XRD patterns are presented in Figure .1. All the samples exhibit a characteristic fluorite structure. A gradual enlargement in the XRD peaks

for all the samples was observed with increase in cobalt concentration. In general, broadening of peaks indicates the reduction in crystallite size. Diffraction pattern of all the Co co-doped powders were observed similar to that of $Ce_{0.9}Gd_{0.1}O_{2-\delta}$ and $Ce_{0.9}Nd_{0.1}O_{2-\delta}$ nanocomposites. No extra peaks were observed for Gd_2O_3, Gd_2O_3 or Co_2O_3. This indicates that cobalt ions have properly dissolved in $Co_yGd_{x-y}Ce_{1-x}O_{2-\delta}$ and $Co_yNd_{x-y}Ce_{1-x}O_{2-\delta}$ (y = 0.05 and 0.1 mol%) systems into the Gd and Nd sites and homogeneous solid solution had formed. It is generally accepted that synthesis of ceramics by wet-chemical method is preferred to those employing reaction in the solid state, because it gives rise to more homogeneous powders with controlled composition. The crystallite size (*D*) was calculated using Scherrer equation

$$D = \frac{0.9\lambda}{\beta cos\theta} \qquad \text{(Equation 1)}$$

Where, *D* is crystallite size, λ is wavelength of X-rays (1.5418Å), θ is the scattering angle of the main reflection and β is the corrected peak at full width at half-maximum (FWHM) intensity.

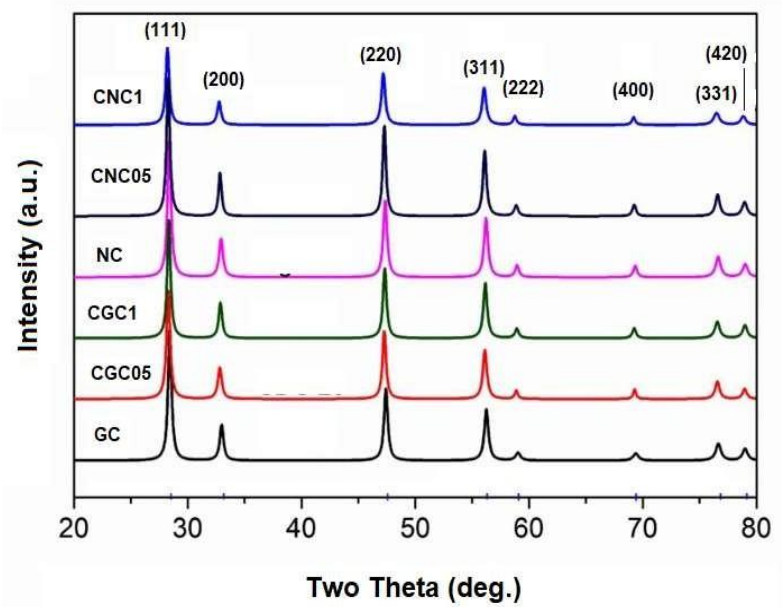

Figure : (1) XRD pattern of cobalt co-doped GDC and NDC nanocomposites.

A slight shift in the peak (1 1 1) towards the lower Bragg's angle, was observed of the obtained data. This shift is caused by the addition of the co-dopant species. The shift is towards the lower Bragg's angle in the case of the Gd and Nd dopants depends on lattice expansion and contraction; when Ce^{4+} (Ionic radii = 97 pm) is doped with higher ionic radii [31] Gd^{3+} (Ionic radii = 107.8 pm) and Nd^{3+} (111 pm), lattice expands, and the peak shift is slight to the left. XRD data presented that, on addition of co-dopant, the (111) peak shifts towards higher Bragg's angle. This shift towards higher Bragg's angle is due to the lattice contraction i.e. when Ce^{4+} ions is substituted with the ion of lower ionic radii Co^{3+} (Ionic radii = 68.5 pm).

Figure.2 shows the effect of cobalt concentration on the average crystallite size of the as-prepared samples calcined at 650°C. One can see that the crystallite size (calculated from Scherrer equation) decreases with increase in the cobalt concentration. Table.1 shows the lattice parameter (a) and the average crystallite size (D) of the samples synthesized by EDTA-Glycol method. It was found that the unit-cell lattice parameter of $Ce_{0.9-x}Co_xSm_{0.1}O_{2-\delta}$ solid electrolytes decreases steadily with increase of cobalt concentration as shown in Figure.3. Such a decrease in unit-cell parameter can be considered to be due to the replacement of bigger Ce^{4+} ions (97 pm) by the smaller Co^{3+} ions (68.5 pm).

International Journal of Environmental Sciences
ISSN: 2229-7359
Vol. 11 No. 21s, 2025
https://www.theaspd.com/ijes.php

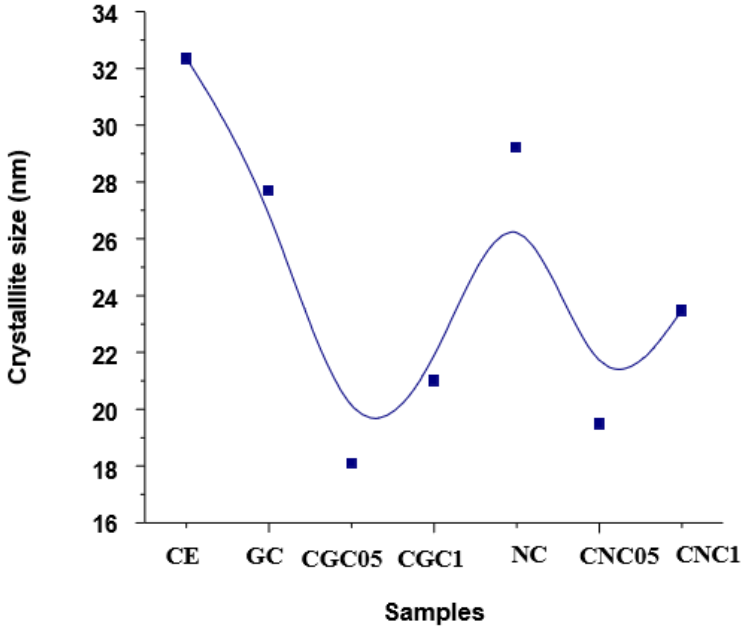

Figure : (2) Effect of Co co-doping on crystallite size of ceria-based materials.

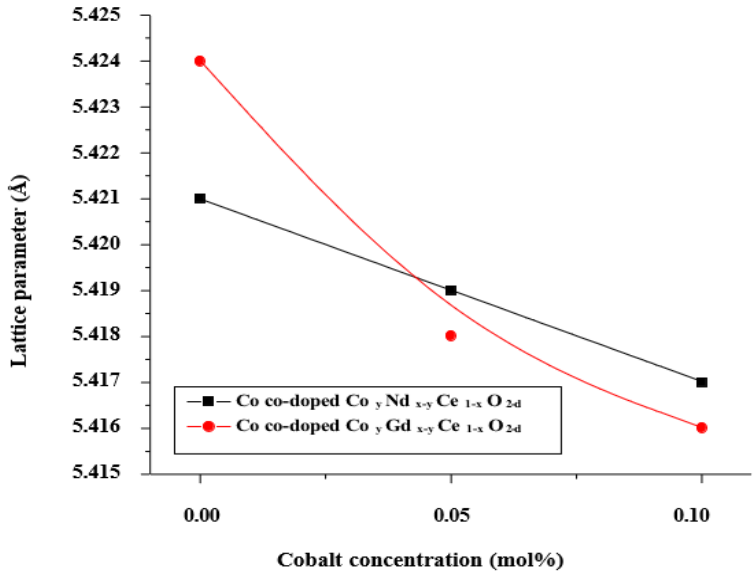

Figure : (3) Effect of cobalt co-doping on lattice parameters of ceria- based nanocomposites.

Table : (1) Lattice parameter (Å), average crystallite size (*D*), relative density, specific surface area (S_{BET}) & average particle sizes (*DBET*) of $Ce_{0.9-x}Co_xSm_{0.1}O_{2-\delta}$ electrolytes.

Sample	Lattice parameter (Å)	Crystallite size, D (nm)	Relative density (%)	*SBET* (m^2/g)	*DBET* (nm)
CE	5.425	32.34	68.45	28.53	29.70
GC	5.421	27.67	97.51	34.11	27.10
CGC05	5.419	18.09	99.34	55.80	13.5
CGC1	5.417	21.00	99.05	49.32	16.2
NC	5.420	29.21	99.42	32.54	19.47
CNC05	5.418	19.47	99.17	52.47	17.91
CNC1	5.416	23.46	99.19	47.63	18.42

The relative densities of CE, GC, CGC05, CGC1, NC, CNC05 and CNC1 samples was obtained at sintered temperatures 1150°C and 1250°C and are presented in Table.1. It is noticed that with increase in sintering temperature, the relative densities of cobalt co-doped ceria- based materials increased from 68.54% to over 99%.

3.2 SEM

Figure .4 (A) shows SEM micrographs of CGC1 and CNC1 samples obtained at 650°C. It can be seen that the co-doped ceria powder calcined at 650°C displayed morphology with random sized particles. Figure .4(B) shows micrographs of thermally etched samples at 1250°C. Micrographs of the surface of the sintered samples show well-defined grains separated by grain boundaries. The samples sintered at 1250°C shows no porosity. No pores are observed on the sample surface, which is consistent with the measured density of the sintered pellet.

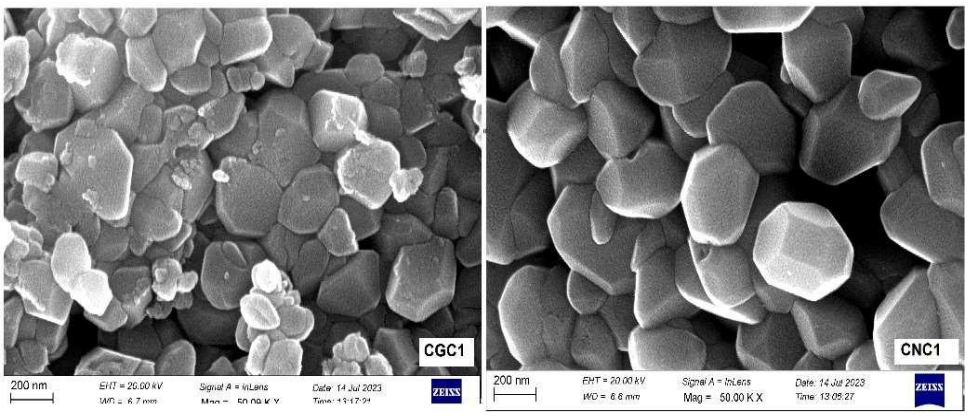

Figure: (4) (A) SEM images of samples CGC1 and CNC1 obtained at 650°C.

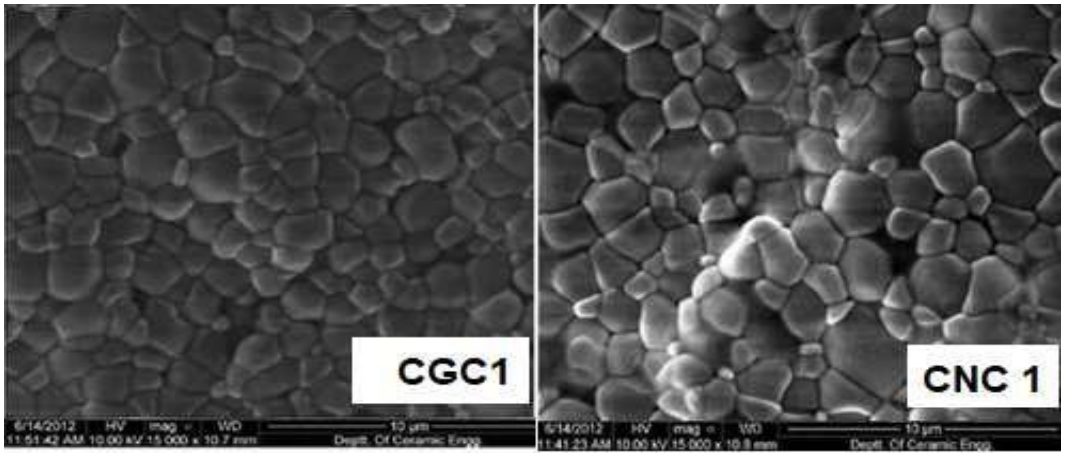

Figure : (4) (B) SEM images of samples CGC1 and CNC1 sintered at 1250°C.

3.3 BET

The specific surface area values are presented in Table.1. The specific area was converted to particle size ($DBET$) according to (Equation 2). From XRD results as well as BET measurements, it is clear that with increasing the concentration of cobalt, particle and crystallite sizes decrease, while the specific surface area increases. The possible reason behind this could be the reduction in the rate of crystal growth in ceria particles caused by the incorporation of cobalt ions in to cubic lattice of $Co_yGd_{x-y}Ce_{1-x}O_{2-\delta}$ and $Co_yNd_{x-y}Ce_{1-x}O_{2-\delta}$ nanocomposites.

$$DBET = \frac{6x10^3}{Dth\, S_{BET}} \quad \text{(Equation 2)}$$

Where, Dth is the theoretical density of sample (g/cm^3) and $DBET$ is the average particle size (nm).

3.4 Ionic conductivity

Conductivity of doped ceria in air has been reported to be completely ionic in nature [34]. In this investigation, the conductivity of samples was measured in air can be treated as oxide ion conductivity. Electrical conductivity of the samples was studied using impedance analysis.

Figure.5 presents the Nyquist plots of the CE, GC, CGC05, CGC1, NC, CNC05 and CNC1 samples at 300°C. From Figure.5, it is clear that two arcs are clear and one arc is not clear. The splitting of curves depends on the

sample nature, temperature, and applied frequency. The left side high-frequency curve is known as the grain resistance, *R*g, the middle region medium frequency curve is the grain boundary resistance, *R*gb, and the right side low-frequency curve is the electrode resistance. In the present study, electrode resistance is not considered for total resistance calculation. It can be further noticed that the depressed semi-circles are present due to the non-uniform distribution of the grains in the sample microstructure which corelates with SEM micrographs. The total resistance is calculated by fitting the Nyquist plots using Zsimpwin software. The equivalent circuit models were employed to fit the Nyquist plots; here, the constant phase element is used instead of a capacitor due to the presence of depressed semi- circles in impedance plots.

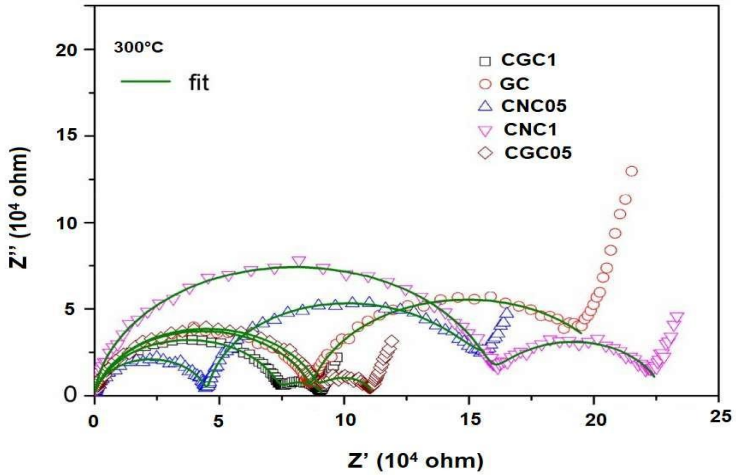

Figure : (5) Nyquist plots of CE, CGC05, CGC1, CNC05, CNC1 samples at 300°C

It is observed that the CE, GC, CGC05, CGC1 and CNC05 samples exhibited lower total resistance whereas higher resistance was observed for the sample CNC1. These results can be correlated with microstructure, i.e. grain size. The sample CGC1 exhibits a lower grain boundary resistance than the rest due to higher density. Similarly, other samples' grain and grain boundary resistance changed with the grain size.

The temperature dependent conductivity of $Co_yGd_{x-y}Ce_{1-x}O_{2-\delta}$ and $Co_yNd_{x-y}Ce_{1-x}O_{2-\delta}$ electrolytes sintered at 1250°C was obtained by plotting a logarithmic relationship between log(σT) and 1000/T (K^{-1}) as shown in Figure.6. However, the electronic conductivity of ceria can be significantly reduced upon the substitution of metal ions. The electrical conductivity of doped ceria is influenced by several factors, such as the dopant ion, the concentration of dopant ion, the oxygen vacancy concentration and enthalpy associated to defects. In this chapter the conductivity of the co-doped samples was measured in air and treated as oxide ionic conductivity. It was found that, the total conductivity of the sintered $Co_yGd_{x-y}Ce_{1-x}O_{2-\delta}$ and $Co_yNd_{x-y}Ce_{1-x}O_{2-\delta}$ (y = 0.05 and 0.1 mol%) samples. followed the order: CGC10 > CNC05 > CGC05 > CNC10.

A Usually, the oxygen vacancies are created due to substitution caused by co-dopant ions which increases the ionic conductivity. In order to introduce mobile oxygen vacancies into the ceria-based compounds, tri- or divalent dopants are added. One possible explanation for the increased conductivity with cobalt concentration is that cobalt ions incorporated into the lattice of $Co_yGd_{x-y}Ce_{1-x}O_{2-\delta}$ and $Co_yNd_{x-y}Ce_{1-x}O_{2-\delta}$ to create oxygen vacancies. The activation energy for conduction is obtained by plotting the ionic conductivity data in the Arrhenius relation for thermally activated conduction. Activation energy can be calculated following the Arrhenius equation (Equation 3):

$$\sigma_t T = \sigma_o \exp\left(\frac{E_a}{kT}\right) \qquad \text{(Equation 3)}$$

where E_a is the activation energy for conduction, T is the absolute temperature, k is the Boltzmann constant and σ_0 is a pre-exponential factor. The equation can be linearised by plotting a logarithmic relationship between log($\sigma_t T$) and 1000/T (K^{-1}).

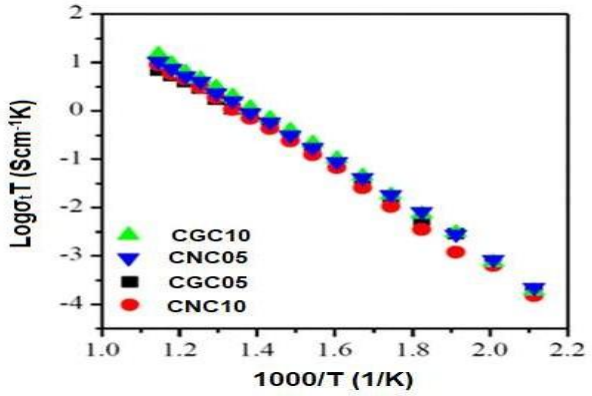

Figure: (6) Arrhenius plots for total ionic conductivity of as-prepared samples.

Values of σ_t at 600°C for different compositions are given in Table.2. Values of σ_t increase with increasing cobalt content up to 0.1 mol% in Gd-doped ceria. First is the ordering of oxygen vacancies is suppressed due to co-doping reported by Yamamura et al. [55]. This decreases the activation energy for migration of O^{2-} ion, consequently increasing the conductivity. Second is due to scavenging effect of grain boundaries by cobalt co-doping leading to increase in the grain boundaries as well as total conductivity. Third is that the ionic size mismatch between Co^{3+} (68.5 pm) and Ce^{4+} (97 pm) [56]. Whereas, in case of cobalt co-doping in Nd-doped ceria, the higher conductivity was observed at lower cobalt content 0.05 mol% (Table.2). Further studies on the reasons for the decrease in the ionic conductivity of cobalt co- doped CNC than compared to undoped NC would be the topic of the future research.

Table: (2) Total conductivity and activation energy of cobalt co-doped ceria.

Sample	Total conductivity (Scm^{-1})	Activation energy (eV)
CGC05	0.0116	0.97
CGC1	0.0168	0.94
CNC05	0.0134	0.95
CNC1	0.0108	0.98

Mainly, the conductivity of ceria-based compounds in air is due to oxide ionic conductivity and the contribution of an electronic conductivity is negligible [34]. On formation of mobile oxygen vacancies, the ionic conductivity dominates the electronic conductivity. It was observed that the oxide ion mobility increases with increasing temperature which in turn increases the conductivity at high temperatures. The activation energy for conduction is obtained by plotting the ionic conductivity data in Equation.2. Figure .7 shows the variation of activation energy with cobalt concentration in as-prepared ceria-based samples. One can see that, as the concentration of cobalt increases from x = 0.05 to 0.1 mol% for Gd-doped ceria, activation energy tends to decrease from 0.96 to 0.94 eV. The minimum value of activation energy (0.94 eV) was observed for the composition $Co_{0.1}Gd_{0.1}Ce_{0.8}O_{2-\delta}$. Such a decrease in activation energy is attributed due to the presence of attractive interactions between dopant cations and oxygen vacancies. For the cobalt concentration x = 0.1 mol% in $Co_yNd_{x-y}Ce_{1-x}O_{2-\delta}$ electrolytes, the activation energy increases (0.98) causing the reduced oxygen ionic conductivity. The ionic conductivity depends mainly on the mobile oxygen concentration. At higher dopant concentration, the reduced ionic conductivity is the result of the formation of local defect structure [11] and lowering in mobile oxygen vacancy concentration.

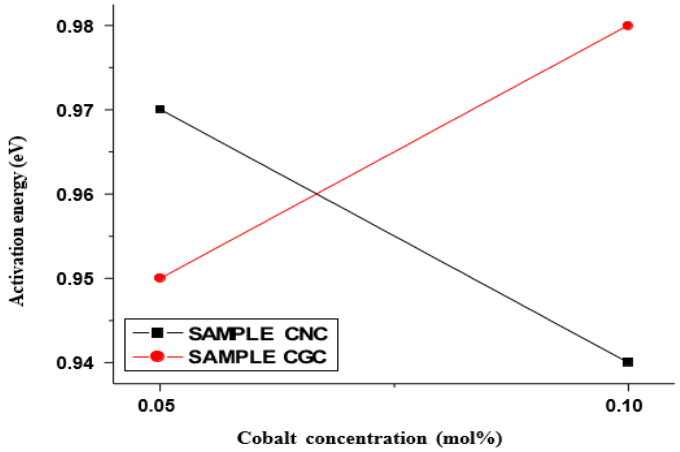

Figure: (7) Effect of cobalt co-doping on activation energy (eV) of as- prepared ceria-based samples.

4.CONCLUSIONS

In summary, the solid solution with compositions $co_ygd_{x-y}ce_{1-x}o_{2-\delta}$ and $co_ynd_{x-y}ce_{1-x}o_{2-\delta}$ (y = 0.05 and 0.1 mol%) were successfully prepared by edta-glycol method. The crystal structure of all the samples calcined at 650°c was fluorite. The calculated crystallite size obtained from xrd and bet have the diameters in the range of 18-32 nm. A relative density of more than 97.50 % is achieved at comparatively reduced sintering temperature of 1250°c. Additionally, cobalt co-doped $co_ynd_{x-y}ce_{1-x}o_{2-\delta}$ sample showed a fairly high ionic conductivity of 0.0166 scm^{-1} at 600°c in air which further demonstrates the use of this material as electrolyte for it-sofcs.

5.REFERENCES

[1] Minh, N.Q.: Ceramic Fuel Cells", J.Am.Ceram.Soc.,76, 563-588, 1993.
[2] Zha, S., Xia, C., Meng, G.: Effect of Gd (Sm) doping on properties of ceria electrolyte for solid oxide fuel cells", J. Power sources 115, 44-48, 2003.
[3] Wei, X., Pan, W., Cheng, L., Li, B.: Atomistic calculation of association energy in doped ceria", Solid State Ionics, 180, 13-17, 2009.
[4] Yahiro, H., Eguchi, Y., Eguchi, K., Arai H.: Oxygen ion conductivity of the ceria-samarium oxide system with fluorite structure", J. Appl. Electro- Chem., 18, 527-531, 1988.
[5] Kochi, E.: Ceramic materials containing rare earth oxides for solid oxide fuel cell", J. Alloys and Compounds, 250, 486-491, 1997.
[6] Bryan, G., Glass, R.S.: ac impedance studies of rare earth oxide doped ceria", Solid State Ionics, 76, 155-162, 1995.
[7] Wang, F. Y., Chen, S., Ccheng, S.: Gd^{3+} and Sm^{3+} co-doped ceria electrolytes for intermediate temperature solid oxide fuel cells", J. Electrochem Commun., 6, 743—746, 2004.
[8] Ralph, J.M., Przydatek, J., Kilner, J.A., Seguelong, T.: Novel doping system in ceria", Ber. Bunsenges. Phys. Chem., 101, 1403-1407, 1997.
[9] Yoshida, H., Deguchi, H., Miura, K., Horiuchi, M.: Investigation of the relationship between the ionic conductivity and the local structures of singly and doubly doped ceria compounds using EXAFS measurement", Solid State Ionics, 140, 191-199, 2001.
[10] Mori, T., Drennan, J., Lee, J.H., Li, J.G., Ikegami, T.: Oxide ionic conductivity and microstructures of Sm- or La-doped CeO2-based systems", Solid State Ionics, 154-155, 461-466, 2002.
[11] Yoshida, H., Inagaki, T., Miura, K., Inaba, M., Ogumi, Z.: Density functional theory calculation on the effect of local structure of doped ceria on ionic conductivity", Solid State Ionics, 160, 109-116, 2003.
[12] Jaiswala, N.; Tanwarb, K.; Sumana, R.; Uppadhyac, D.K.S.; Parkash, O. A Brief Review on Ceria Based Solid Electrolytes for Solid Oxide Fuel Cells. *J. Alloys Compd.* 2019, *781*, 984–1005.
[13] Santos, T.H.; Grilo, J.P.F.; Loureiro, F.J.A.; Fagg, D.P.; Fonseca, F.C.; Macedo, D.A. Structure, densification and electrical properties of Gd^{3+} and Cu^{2+} co-doped ceria solid electrolytes for SOFC applications: Effects of Gd2O3 content. *Ceram. Int.* 2018, *44*, 2745–2751.
[14] Anwar, M.; Muhammad Ali, S.A.; Muchtar, A.; Somalu, M.R. Influence of strontium co-doping on the structural, optical, and electrical properties of erbium-doped ceria electrolyte for intermediate temperature solid oxide fuel cells. *Ceram. Int.* 2019, *45*, 5627–5636.
[15] Liu, Y.; Mushtaq, M.N.; Zhang, W.; Teng, A.; Liu, X. Single-phase electronic-ionic conducting $Sm^{3+}/Pr^{3+}/Nd^{3+}$ triple-doped ceria for new generation fuel cell technology. *Int. J. Hydrog. Energy* 2018, *43*, 12817– 12824.
[16] Holtappels P, Poulsen FW, Mogensen M (2000) Electrical conductivities and chemical stabilities of mixed conducting pyrochlores for SOFC applications. Solid State Ionics 135:675–679.
[17] Tuller HL, Tuller H, Schoonman J, Riess I (2000) Oxygen ion and mixed conductors and their technological applications. In: Riess I (ed) Defects and transport. Kluwer (NATO ASI series), Dordrecht, pp 245– 270.
[18] Etsell H, Flengas SN (1970) The electrical properties of solid oxide electrolytes. Chem Rev 70:339–376.

[19] Rickert H (1982) Electrochemistry of solids—an introduction, Springer-Verlag, Berlin.
[20] Chebotin VN, Perfilyev MV (1978) Electrochemistry of solid electrolytes. Khimiya, Moscow.
[21] Perfilyev MV, Demin AK, Kuzin BL, Lipilin AS (1988) High temperature electrolysis of gases. Nauka, Moscow.
[22] Kharton VV, Naumovich EN, Vecher AA (1999) Research on the electrochemistry of oxygen ion conductors in the former Soviet Union I ZrO2-based ceramic materials. J Solid State Electrochem 3:61–81.
[23] Inaba H, Tagawa H (1996) Ceria based electrolytes. Solid State Ionics 83:1–16 [35] Bouwmeester HJM, Burggraaf AJ(1996) In: Burggraaf A, Cot L (eds) Fundamentals of inorganic membrane science and technology. Elsevier, Amsterdam, pp 435–528.
[24] Sammes NM, Tompsett GA, Nafe H, Aldinger F (1999) Bismuth based oxide electrolytes—structure and ionic conductivity. J Eur Ceram Soc 19:1801–1826.
[25] Mogensen M, Sammes NM, Tompsett GA (2000) Physical chemical and electrochemical properties of pure and doped ceria. Solid State Ionics 129:63–94.
[26] Mori T, Drennan J, Lee JH, Li JG, Ikegami T (2002) Solid State Ionics 154–155:461.
[27] Van Herle J, Seneviratne D, McEvoy A J (1999) J Eur Ceram Soc 19:837.
[28] Shannon RD. Revised effective ionic radii and systematic studies of interatomic distances in halides and chalcogenides. Acta Crystallogr A. 1976;32(5):751–767.
[29] Inaba H, Tagawa H (1996) Ceria based electrolytes. Solid State Ionics 83:1–16
[30] Yamamura H, Katoh E, Ichikawa M, Kakinuma K, Mori T, Haneda H (2000) Multiple doping effect on the electrical conductivity in the $(Ce_{1-x-y}La_xM_y)O_{2-\delta}$ (M=Ca, Sr) system. Electrochemistry 68:455–459.
[31] Kim DK, Cho PS, Lee JH, Kim DY, Park HM, Auchterlonie G et al (2007) Mitigation of highly resistive grain-boundary phase in gadolinia- doped ceria by the addition of SrO. Electrochem Solid State Lett 10:B91– B95.